Human Molecular Genetics, 2012, Vol. 21, No. 18 **3956–3968**
doi:10.1093/hmg/dds210
Advance Access published on June 1, 2012

A persistent level of Cisd2 extends healthy lifespan and delays aging in mice

Chia-Yu Wu[1,†], Yi-Fan Chen[5,†], Chih-Hao Wang[2,†], Cheng-Heng Kao[6], Hui-Wen Zhuang[1], Chih-Cheng Chen[7], Liang-Kung Chen[3,8], Ralph Kirby[1], Yau-Huei Wei[2,9], Shih-Feng Tsai[1,5] and Ting-Fen Tsai[1,3,4,5,*]

[1]Department of Life Sciences and Institute of Genome Sciences, [2]Institute of Biochemistry and Molecular Biology, [3]Aging and Health Research Center and [4]VGH-YM Genome Research Center, National Yang-Ming University, Taipei 112, Taiwan [5]Institute of Molecular and Genomic Medicine, National Health Research Institutes, Zhunan, Miaoli County 350, Taiwan, [6]Center of General Education, Chang Gung University, Taoyuan 333, Taiwan, [7]Institute of Biomedical Sciences, Academia Sinica, Taipei 115, Taiwan, [8]Center for Geriatrics and Gerontology, Taipei Veterans General Hospital, Taipei 112, Taiwan and [9]Department of Medicine, Mackay Medical College, New Taipei City 252, Taiwan

Received February 10, 2012; Revised April 15, 2012; Accepted May 28, 2012

The *CISD2* gene, which is an evolutionarily conserved novel gene, encodes a transmembrane protein primarily associated with the mitochondrial outer membrane. Significantly, the *CISD2* gene is located within the candidate region on chromosome 4q where a genetic component for human longevity has been mapped. Previously, we have shown that Cisd2 deficiency shortens lifespan resulting in premature aging in mice. Additionally, an age-dependent decrease in Cisd2 expression has been detected during normal aging. In this study, we demonstrate that a persistent level of Cisd2 achieved by transgenic expression in mice extends their median and maximum lifespan without any apparent deleterious side effects. Cisd2 also ameliorates age-associated degeneration of the skin, skeletal muscles and neurons. Moreover, Cisd2 protects mitochondria from age-associated damage and functional decline as well as attenuating the age-associated reduction in whole-body energy metabolism. These results suggest that Cisd2 is a fundamentally important regulator of lifespan and provide an experimental basis for exploring the candidacy of CISD2 in human longevity.

INTRODUCTION

Since the beginning of time, humans have been searching for the secrets of the fountain of youth in order to promote longevity and help maintain quality of life in the old age. In addition to environmental factors such as nutrition control of diet and caloric restriction that can modulate lifespan, there is substantial evidence to support the familial aggregation of exceptional longevity in humans, which suggests that there is a genetic factor or factors associated with a long life. Thus, researchers have been wondering whether the fountain of youth has indeed a genetic component and does it stream from hundreds/thousands of genes, or only a very few?

In 2001, Perls, Kunkel and their colleagues conducted an open-ended search designed to pick up any genetic region that confers exceptional longevity in humans. They carried out a genome-wide scan of long-lived families using 308 individuals who belonged to 137 sets of extremely old siblings; this linkage study identifies a locus on chromosome 4q and suggests that there is a genetic component that contributes significantly to longevity (1). Although there are many articles that have examined the process of aging in a variety of experimental organisms, it is extremely valuable to obtain information that relates to humans. Accordingly, the linkage study of long-lived sibling pairs in humans represents a significant advance (1), because it points toward an area for further

*To whom correspondence should be addressed at: Department of Life Sciences and Institute of Genome Sciences, National Yang-Ming University, 155 Li-Nong St., Sec. 2, Peitou, Taipei 112, Taiwan. Tel: +886 228267293; Fax: +886 228280872; Email: tftsai@ym.edu.tw
†The authors wish it to be known that, in their opinion, the first three authors should be regarded as joint First Authors.

exploration. However, the suspect region on chromosome 4q spans ~12 Mb and contains hundreds of candidate genes. Until now, the genetic component on chromosome 4q that may confer human lifespan control has remained unclear.

The CDGSH iron–sulfur domain-containing protein 2 (*CISD2*; synonym: *Miner 1*, *Naf-1*, *ERIS*, *Noxp70* and *ZCD2*) gene is an evolutionarily conserved gene (2). Significantly, the *CISD2* gene is located within the candidate region on chromosome 4q where a genetic component for human longevity has been mapped. Additionally, the *CISD2* gene has also been identified as the causative gene for Wolfram syndrome 2 (MIM 604928), which is an autosomal-recessive neurodegenerative disorder (3). Previous study of its crystal structure has shown that Cisd2 is a homodimer harboring two redox-active 2Fe–2S clusters (4). Recent studies have suggested that Cisd2 may function as an autophagy regulator and may be involved in the Bcl-2-mediated regulation of autophagy and calcium homeostasis (5,6). We had engineered Cisd2-deficient knockout (KO) mice in order to study the role of Cisd2 in development and pathophysiology. Early senescence is accompanied by a shortened lifespan in the Cisd2 KO mice and there appears to be signs of haplo-insufficiency in heterozygous mice. In addition, these mutant mice exhibit an accelerated aging phenotype with 100% penetrance for both sexes (7,8). The *Cisd2* gene encodes a transmembrane protein primarily associated with the mitochondrial outer membrane. Our results revealed that Cisd2 deficiency leads to mitochondrial degeneration accompanied by cell death that has autophagic features. Since mitochondria are the cellular energy factories that generate ATP via oxidative phosphorylation, this degeneration has direct functional consequences and leads to respiratory dysfunction (7,8). Our results thus provide strong evidence for the causal involvement of mitochondrial dysfunction in driving mammalian aging.

Many genetic factors have the potential to modulate lifespan (9–13). However, so far, *Cisd2* is the only identified gene that resides in the longevity region of 4q and has been demonstrated to be an essential gene for lifespan control by a loss-of-function mouse study. Nonetheless, experiments that shorten lifespan are likely to be less informative than those that prolong a healthy lifespan. Accordingly, it is very interesting and important to evaluate the life history of transgenic (TG) mice expressing an elevated level of the Cisd2 protein in order to see whether increased Cisd2 promotes longevity. In this study, we create a Cisd2 TG mouse model that is able to provide gain-of-function evidence, demonstrating that elevated expression of Cisd2, specifically a persistent level of Cisd2 during middle and old age, extends the healthy lifespan of mice and delays age-associated phenotypes in mice.

RESULTS

Cisd2 promotes longevity

To study whether enhanced expression of Cisd2 can extend lifespan, delay aging and help to retain the functional abilities lost with age, we generated Cisd2 TG mice carrying the *Cisd2* coding region controlled by the RNA polymerase II large subunit (Pol II) promoter in a C57BL/6 mouse background (Fig. 1A). RNA analysis revealed a similar pattern for the endogenous and TG Cisd2 mRNA expression using northern blot hybridization (Fig. 1B). In wild-type (WT) mice, the levels of Cisd2 decrease in an age-dependent manner during aging (2). In the present study, we show that there is an average 38 and 57% decrease in the Cisd2 protein level in skeletal muscle of WT mice at middle age (12-month-old; 12-mo) and old age (24-mo), respectively, compared with young (3-mo) mice; however, in Cisd2 TG mice, there is a persistent expression level of the Cisd2 protein from young (3-mo) through middle age (12-mo) to old age (24-mo) (Fig. 1C). In the brain and skin, similar results were obtained for the age-dependent decrease in Cisd2 in the WT mice, whereas a persistent expression level of the Cisd2 protein in these tissues of the Cisd2 TG mice was observed as the mice aged (Supplementary Material, Fig. S1A and B). It appears that the TG Pol II promoter exhibited constitutive activity during aging when driving Cisd2 expression.

An extended lifespan was evident for both sexes of the Cisd2 TG mice without any statistically significant sex differences (Table 1). In males (Fig. 1D, Table 1), the median lifespan of the Cisd2 TG mice was increased by 5.25 months (19.4%; from 27 months to 32.25 months) relative to WT mice ($P < 0.001$), whereas the maximum lifespan (mean lifespan of the oldest 10% within a cohort) was increased by 3.66 months (11.7%; $P = 0.043$). In females (Fig. 1E, Table 1), the median lifespan in Cisd2 TG mice was increased by 5.1 months (18.8%; from 27.15 to 32.25 months) relative to WT mice ($P < 0.001$), whereas the maximum lifespan was increased by 8.75 months (29.6%; $P = 0.032$).

According to evolutionary theory, in particular, the disposable soma theory, the maximum fitness of an organism is a trade-off between fertility and longevity (14,15). The long-lived Klotho TG mice provide an example of this inverse correlation between fertility and lifespan (16). Furthermore, the cost of reproduction is higher for females than for males due to the energetic and nutritional requirements of pregnancy and lactation (17). To detect possible effects of constitutive Cisd2 expression on reproductive phenotypes, we performed a breeding test using Cisd2 TG females. The numbers of litters and pups as well as the litter size were recorded from 2-mo to 12-mo for each female. Our results revealed no obvious difference in female fertility between the WT and Cisd2 TG mice (Supplementary Material, Fig. S2A). In addition, there was no obvious phenotypic effect on body weight or body temperature when the Cisd2 TG mice were compared with WT mice (Supplementary Material, Fig. S2B and C). Additionally, we measured the metabolic indices of the Cisd2 TG mice, including intake of food and water and generation of urine and stool. No significant difference in these metabolic indices was observed (Supplementary Material, Fig. S2D). These results suggest that Cisd2 modulates lifespan through mechanisms that are likely to be independent of growth, food intake and reproduction.

Cisd2 delays skin aging

Age-associated structural and functional changes are more visibly evident in the skin than in any other organ in mammals. Interestingly, the fur of a very old (34-mo) Cisd2

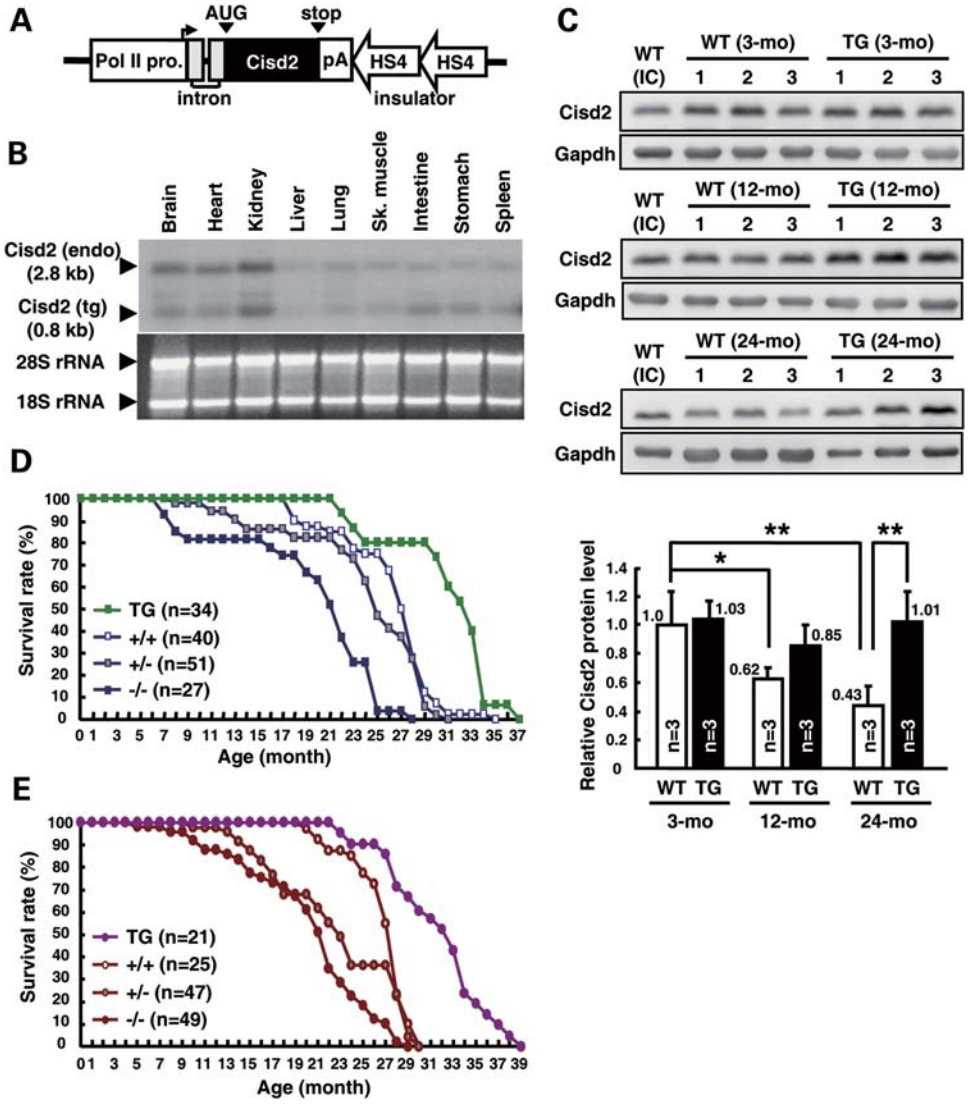

Figure 1. Persistent expression of Cisd2 promotes longevity in mice. (**A**) The Pol II-*Cisd2* TG construct. The mouse *Cisd2* coding region is driven by the RNA polymerase II large subunit promoter (Pol II pro.); two direct repeats of the chicken HS4 insulator were placed downstream of the polyA (pA) signal to block positional effects. The Cisd2 TG mice were generated using a C57BL/6 background. (**B**) Northern blot analysis of the endogenous (endo) and transgenic (tg) Cisd2 mRNA of Cisd2 TG mouse at 3-mo using mouse *Cisd2* cDNA as the probe. (**C**) Western blot analyses and quantification of Cisd2 protein levels in the skeletal muscles for WT and Cisd2 TG mice at 3-mo, 12-mo and 24-mo. The results are shown as the mean ± SD. $^{*}P < 0.05$; $^{**}P < 0.005$. IC, an internal control using the same skeletal muscle sample (WT 12-mo) that allows normalization of the signals between different western blots. (**D**, **E**) Dose-dependent modulation of lifespan by Cisd2 in male and female mice. Cisd2 deficiency shortens the lifespan and causes premature aging in both the male and female *Cisd2* KO mice. In contrast, a persistent level of Cisd2 expression prolongs lifespan and increases the survival rate of both male and female Cisd2 TG mice.

TG mouse appeared to have less grey hairs (de-pigmentation) and to display a more prominent sheen than that of a middle-aged (15-mo) WT mouse (Fig. 2A). Histological examination (Fig. 2B–E) and quantification (Fig. 2F) revealed that age-dependent atrophy of the sebaceous glands, which are the lipid-producing structures associated with the hair follicles, was significantly delayed in Cisd2 TG mice at 24-mo. In addition, the proportion of individual hair follicles associated with two sebaceous glands was significantly increased in the Cisd2 TG mice at 24-mo (Fig. 2G).

Sebaceous glands secrete lipids (sebum) that coats the hair; in furry mammals, these lipids play important roles in water repulsion and thermoregulation (18,19). Sebaceous glands change as skin ages and therefore we tested the ability of different ages of mice to repel water and maintain body temperature when wet. Although the core body temperature after water immersion showed no significant differences between age-matched WT and Cisd2 TG mice (Supplementary Material, Fig. S3A), the water repulsion test revealed an interesting difference. Five minutes after water immersion, young mice at 3-mo from both the WT and Cisd2 TG groups were nearly dry (Fig. 2H). As expected, old mice from the 24-mo WT group, which displayed sebaceous gland atrophy, exhibited impaired water repulsion (Fig. 2H). Remarkably, the ability of old (24-mo) Cisd2 TG mice to repel water was similar to that of young (3-mo) mice (Fig. 2H). Skin aging is also

Table 1. Extended median and maximum lifespan of the Cisd2 TG mice

Genotype	Median	Mean	Maximum	Minimum	Oldest 10%	Youngest 10%	*n*
Male							
Cisd2 TG	32.25	30.72 ± 1.18	36.73	21.73	34.86 ± 1.62	22.51 ± 0.77	34
WT	27	25.74 ± 0.62	34	17.06	31.20 ± 1.93	17.31 ± 0.21	40
Female							
Cisd2 TG	32.25	31.22 ± 0.96	39	22.2	38.35 ± 0.92	22.94 ± 1.04	21
WT	27.15	26.28 ± 0.41	29.8	19.13	29.60 ± 0.28	19.57 ± 0.62	25

Mouse age is presented in months.

associated with a decrease in skin thickness, which is mainly due to atrophy of the subcutaneous fat and muscle; this phenotype was observed in both WT and Cisd2 TG mice at 24-mo (Supplementary Material, Fig. S3B–I). Nevertheless, an increase in hair regrowth rate was observed for the Cisd2 TG mice during middle age (12-mo) (Supplementary Material, Fig. S3J). When taken together, these results revealed that skin aging seems to be significantly delayed by the persistent expression of Cisd2 and, most obviously, Cisd2 alleviates sebaceous gland atrophy during skin aging.

Cisd2 delays muscle aging

Muscle strength declines with aging. Quantitative loss of muscle mass, namely sarcopenia, is the most important factor underlying this phenotype (20). Sarcopenia is accompanied by increased muscle fat infiltration, and the accumulation of fat mass in aged muscle has been shown to be a predictor of subsequent functional loss and disability in humans (21,22). Strikingly, constitutive Cisd2 expression has a profound effect and protects skeletal muscles from age-dependent mass losses and prevents fat infiltration (Fig. 3A–F). Quantification of the phenomena revealed that there was a significant increase in fiber size (Fig. 3G) and fiber number (Fig. 3H), as well as a significant decrease in lipid infiltration (Fig. 3I) in the Cisd2 TG mice at 24-mo. Furthermore, functional muscle strength improvement in the Cisd2 TG mice was demonstrated using a grip strength meter (Fig. 3J). A detailed transmission electron microscopy (TEM) examination further revealed that Cisd2 indeed protects from age-associated degeneration the mitochondria within and the ultrastructure of skeletal muscle, in Cisd2 TG mice, including myofilaments; this is in contrast to the overt mitochondrial degeneration, which is accompanied with autophagy, in the aged muscles of WT mice at 24-mo (Fig. 3K–N).

Cisd2 delays neuron aging

Morphologically, the non-myelinated and myelinated axons, which are enveloped by a myelin sheath formed by the fusion of many layers of plasma membrane from Schwann cells, can be identified using TEM micrography (Fig. 4). Notably, considerable age-associated degeneration of the non-myelinated and myelinated axons as well as the disintegration of the myelin sheath were detected in the sciatic nerve (Fig. 4A and B) and optic nerve (Fig. 4C and D) of aged WT mice at 24-mo. Interestingly, the persistent expression of Cisd2 appears to protect the TG mice from the age-associated damage to both the sciatic (Fig. 4E and F) and optic nerves (Fig. 4G and H). Furthermore, neuron degeneration in the aged WT mice seems, in turn, to lead to a decrease in neuron density, which is supported by our quantification. Our results show that there are striking differences in the numbers of myelinated axons in the sciatic and optic nerves when WT and Cisd2 TG mice are compared, which suggest that Cisd2 appears to protect these nerves (Fig. 4I–L). To examine motor functions in older mice, we assessed behavior using an open-field locomotion test and rotarod trials. There was a trend toward better motor function in the Cisd2 TG mice compared with the age- and sex-matched WT mice at 24-mo (Supplementary Material, Fig. S4).

Cisd2 protects mitochondria from age-associated damage, reduces the age-associated declines in mitochondrial function and whole-body energy metabolism

Since Cisd2 deficiency causes mitochondrial dysfunction and triggers an accelerated aging process in Cisd2 KO mice, we sought to investigate whether an elevated level of the Cisd2 protein was able to protect mitochondria from age-associated damage in Cisd2 TG mice. There is progressive damage to mitochondrial DNA (mtDNA) during aging. To study whether Cisd2 is able to protect mitochondria from age-associated genomic damage, we examined mtDNA integrity by long polymerase chain reaction (PCR; 13.6 kb) of mtDNA (23); this amplification covers >83% of mitochondrial genome (Fig. 5A). DNA polymerase amplifies only undamaged templates, therefore any damage to the mtDNA (such as strand breaks, abasic sites and certain types of oxidative lesions) will block the progression of the DNA polymerase, thus decreasing amplification; in addition, internal mtDNA deletions may yield shorter PCR fragments that can be visualized by gel electrophoresis. Indeed, we detected a reduction in the amplification of the 13.6-kb fragment and an increase in the number of shorter PCR fragments in the old (24-mo) WT mice compared with the young (3-mo) mice (Fig. 5B and C). In contrast, the old (24-mo) Cisd2 TG mice were protected from this age-associated increase in mtDNA damage (Fig. 5B and C). Additionally, PCR amplification of the D-17 deletion, which covers the *ND1* and *ND2* genes (24), revealed that Cisd2 attenuates this age-associated mtDNA deletion in the old (24-mo) Cisd2 TG mice (Fig. 5D and E). Nonetheless, there was no significant difference in D-loop oxidative damage (Supplementary Material, Fig. S5A).

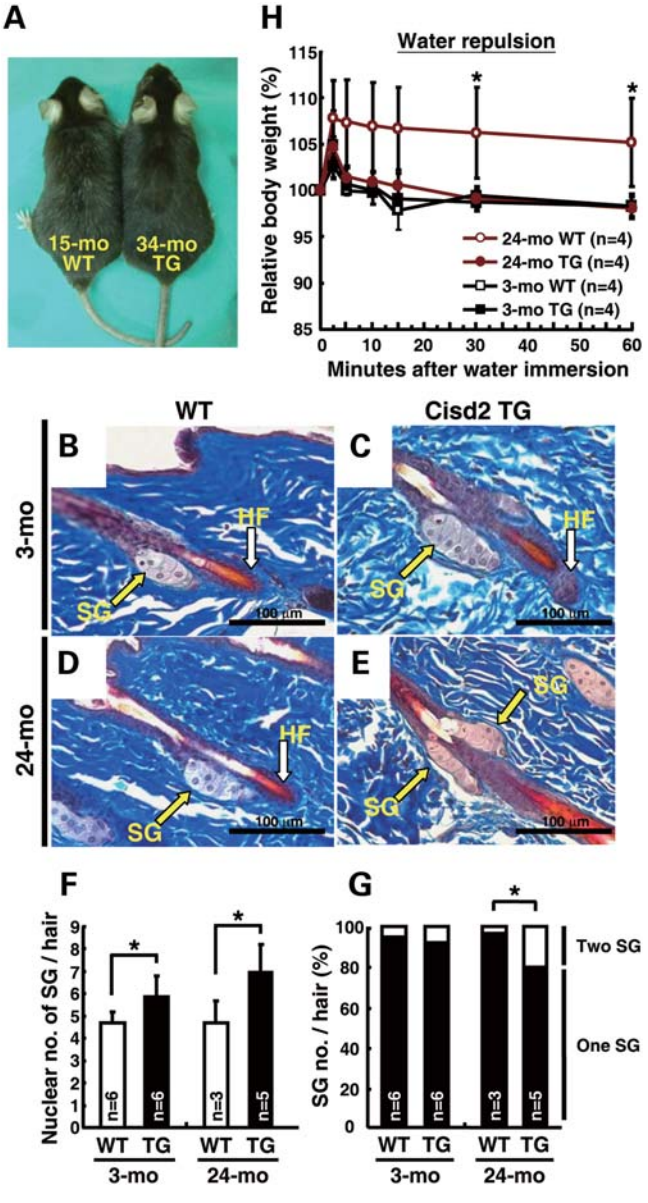

Figure 2. Effects of Cisd2 on fur appearance, sebaceous glands and water repulsion. (**A**) Delayed de-pigmentation in the Cisd2 TG mice. There are less grey hairs present in the 34-mo Cisd2 TG mouse compared with a 15-mo WT mouse. (**B**, **C**) Masson's trichrome staining of skin section for WT and Cisd2 TG mice at 3-mo. HF, hair follicles; SG, sebaceous gland. Connective tissues, principally collagen, are stained blue by Masson's trichrome staining. (**D**, **E**) Masson's trichrome staining of skin sections for WT and Cisd2 TG mice at 24-mo. (**F**) Quantification of nuclear numbers in sebaceous gland per hair. (**G**) Percentage of hairs with one SG or two SG per individual hair. In (F) and (G), there were 3–6 mice in each group; for each mouse, 40–180 hairs were examined. (**H**) Better water repulsion in Cisd2 TG mice at 24-mo. The WT mice retained more water in their fur than did the Cisd2 TG mice, which is reflected as a significant increase in relative body weight. All results are mean ± SD. $^{*}P < 0.05$.

To investigate whether an attenuation of the age-associated damage to mtDNA has a direct functional benefit, we assessed aerobic respiration using isolated mitochondria prepared from skeletal muscle. Our results revealed an age-dependent decrease in oxygen consumption in both the WT and Cisd2 TG mice; however, there was a remarkable increase in the oxygen consumption of the mitochondria from the Cisd2 TG mice compared with those from the WT controls at the old age (24-mo) (Fig. 5F). To further expand this investigation, we measured the enzyme activities of Complexes I and IV, and the electron transport activity of Complexes I–III and Complexes II–III. Our results revealed a significant increase in the activity levels of Complex I and Complexes I–III in the old (24-mo) Cisd2 TG mice compared with the control mice (Fig. 5G–J); this result is consistent with the observation that Cisd2 TG mice have a reduced level of D-17 deletion, which covers the *ND1* and *ND2* genes that encode two components of Complex I (Fig. 5D and E). Previous studies have shown that Complex I is likely to regulate aging process and that a decrease in Complex I activity has been found to be associated with aging (25,26). In Cisd2 TG mice, the attenuation of the D-17 deletion seems to have a direct functional consequence and may contribute to an improvement in the enzyme activity of Complex I and in higher levels of electron transport activity of Complexes I–III during old age. Together, these results show that constitutive expression of Cisd2 protects mitochondria and reduces the age-associated decline in aerobic respiration during aging.

To assess the impact of better preserved mitochondrial function on age-associated changes in whole-body energy metabolism, we monitored the mice by indirect calorimetry. Consistent with the decreased oxygen consumption observed using the isolated mitochondria of old (24-mo) WT mice, whole-body oxygen consumption (VO_2), CO_2 production (VCO_2) and heat generation were significantly decreased in the old (24-mo) WT mice compared with the young (3-mo) WT mice during both light and dark cycles (Fig. 6A–F). In contrast, old (24-mo) Cisd2 TG mice were well protected from these age-associated reductions in O_2 consumption, CO_2 production and heat generation during the light cycle; furthermore, during the dark cycle, although the reduction in these age-associated parameters was not fully protected, the decline was significantly attenuated in the Cisd2 TG mice (Fig. 6D–F). Taken together, these results demonstrate that aging is associated with mitochondrial damage and is accompanied by a reduction in mitochondrial function and whole-body energy metabolism. Importantly, these deleterious changes can be prevented or significantly ameliorated by a persistent level of Cisd2 expression during aging.

To test whether a decrease in oxidative stress contributes to the longevity phenotype of Cisd2 TG mice, we monitored intracellular glutathione (GSH) levels in the skeletal muscles of young (3-mo) and old (24-mo) WT and Cisd2 TG mice; GSH is an important antioxidant involved in defense against oxidative stress and the maintenance of cellular redox homeostasis (27). Our result revealed no significant differences in GSH levels at both young and old ages between WT and Cisd2 TG mice (Supplementary Material, Fig. S5B). In addition, the mRNA levels of the enzymes that scavenge reactive oxygen species (ROSs) were also unaffected (Supplementary Material, Fig. S5C). These findings suggest that modulation of the ROS-induced stress response does not seem to play a significant role in the anti-aging effect of Cisd2 in the TG mice.

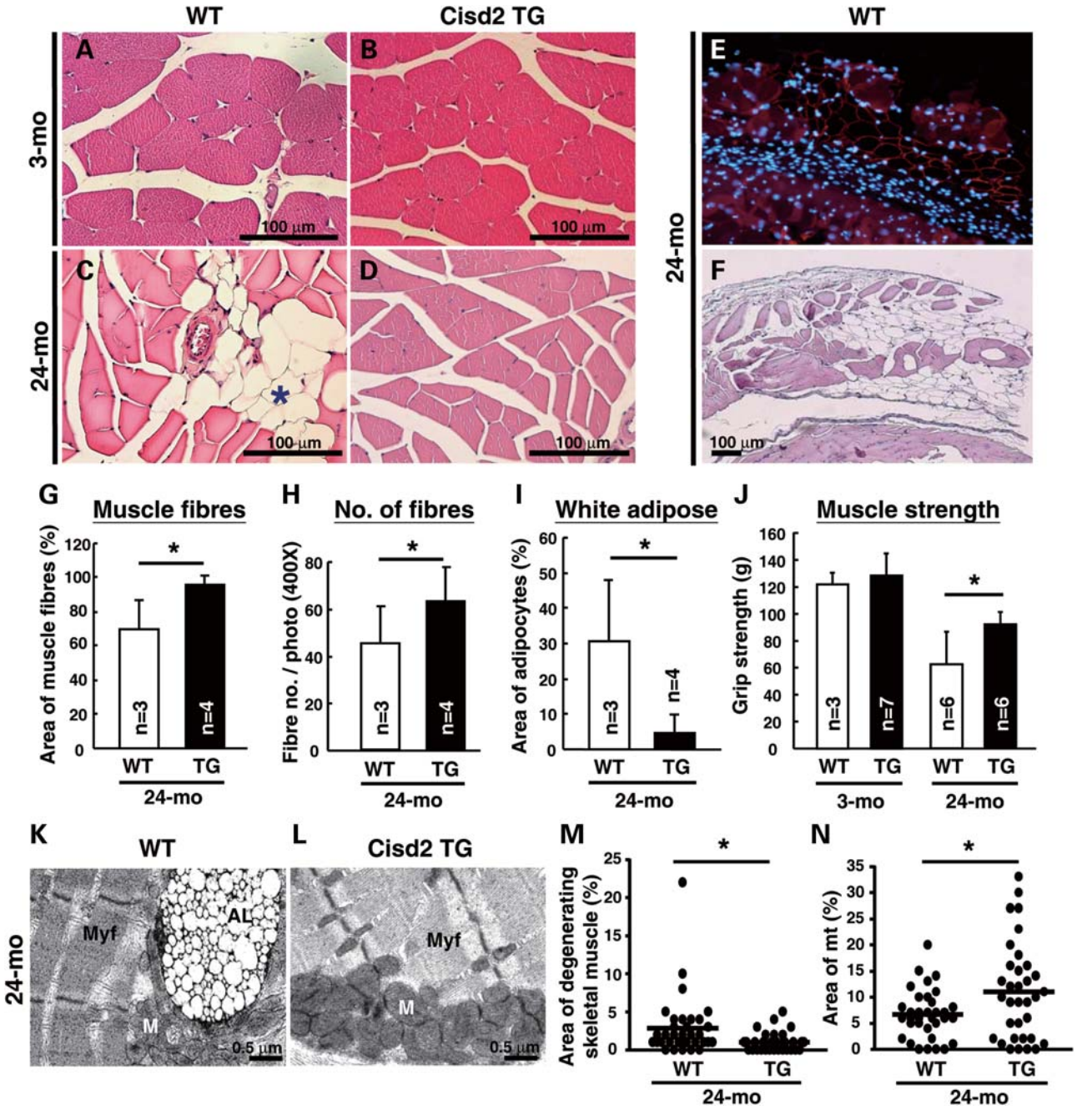

Figure 3. Cisd2 protects mitochondria from age-associated structural damage and delays skeletal muscle degeneration. (**A**–**D**) H&E staining of transverse sections of the skeletal (femoris) muscles from 3-mo WT (A), 3-mo Cisd2 TG (B), 24-mo WT (C), and 24-mo Cisd2 TG (D) mice. Star indicates white adipose tissue substituting for muscle fibers. (**E**) White adipose tissue in the skeletal muscle was confirmed by IHC staining for perilipin which is expressed at the periphery of lipid droplets. The blue color is nuclear staining by DAPI. (**F**) H&E staining of a serial section examined in panel (E). (**G**) Significant increase in the area occupied by muscle fibers in Cisd2 TG mice at 24-mo. (**H**) Significant increase in the fiber numbers in Cisd2 TG mice at 24-mo. (**I**) Significant decrease in the area substituted by white adipocytes in the skeletal muscle of Cisd2 TG mice at 24-mo. In (G)–(I), there were 3–4 mice in each group; 3–5 micrographs (400×) for each mouse were examined. All results are mean ± SD. $^{*}P < 0.05$. (**J**) Functional examination of muscle strength using grip strength analysis. (**K**, **L**) TEM examination of ultrastructure of the skeletal (femoris) muscles at 24-mo. AL, autolysosomes; M, mitochondria; Myf, myofilament. (**M**) Percentage of the skeletal muscle showing degenerative areas and autophagic vacuoles at 24-mo. (**N**) Percentage of area occupied by mitochondria (mt) in the skeletal muscle at 24-mo. In (M) and (N), there were three mice in each group; 10–12 TEM micrographs (5000×) for each mouse were examined. $^{*}P < 0.05$.

DISCUSSION

The central finding in this work is that maintaining a persistent level of Cisd2 expression over the different stages of life promotes longevity and ameliorates age-associated phenotypes in mice. Our observation indicates that Cisd2 is a fundamentally important mediator that is able to regulate lifespan in a mammal. Previously, we have provided evidence demonstrating that Cisd2 deficiency shortens lifespan and drives premature aging

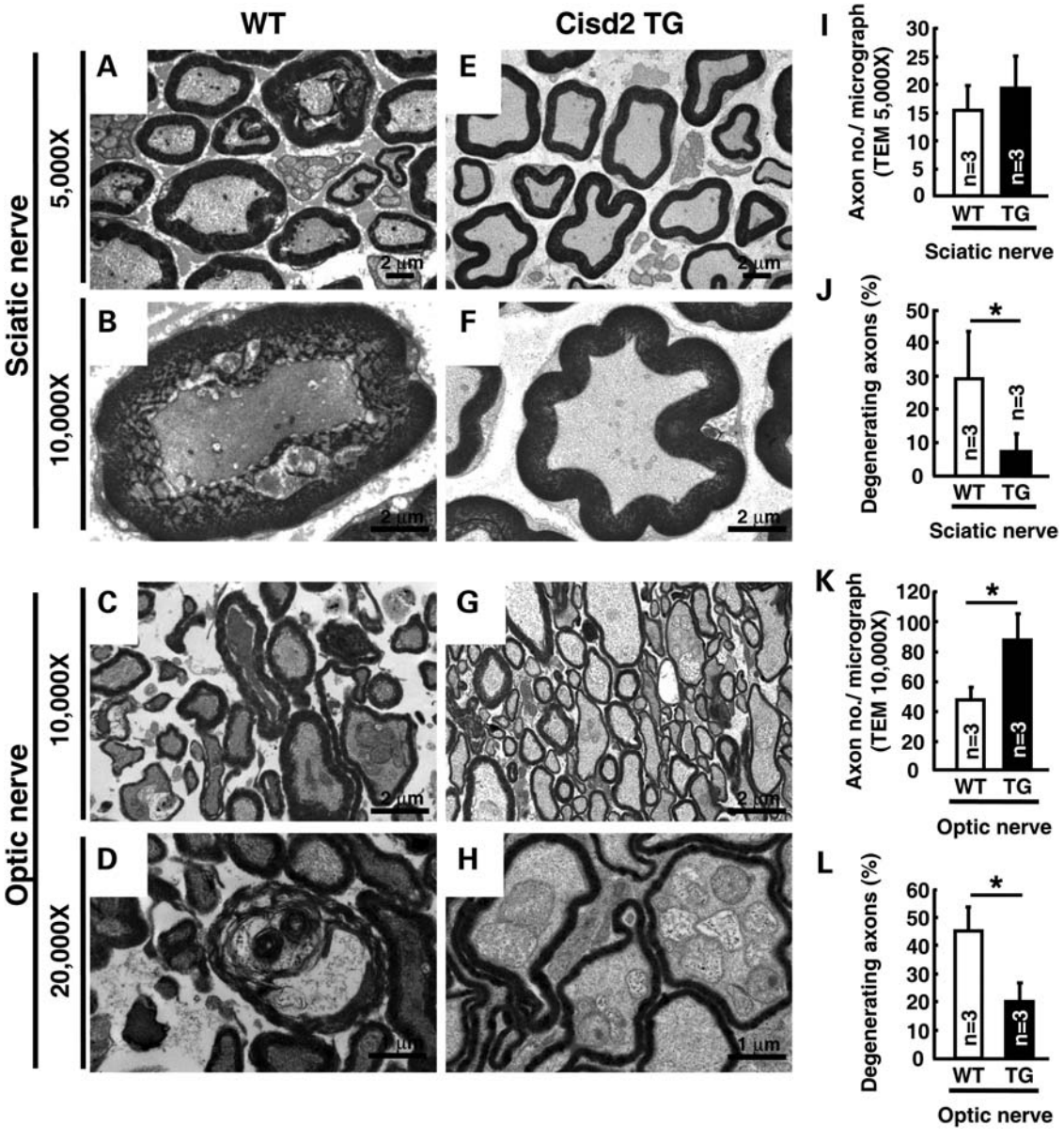

Figure 4. Cisd2 protects mice from age-associated neuron degeneration and myelin sheath disintegration. (**A**, **B**) Ultrastructure of the sciatic nerve of WT mice at 24-mo. Disintegration of the myelin sheath and degenerating axonal components are evident. (**C**, **D**) Ultrastructure of the optic nerve of WT mice at 24-mo. Disintegration of the myelin sheath and degenerating axonal components are evident. (**E**, **F**) Ultrastructure of the sciatic nerve of the Cisd2 TG mice at 24-mo. (**G**, **H**) Ultrastructure of the optic nerve of the Cisd2 TG mice at 24-mo. (**I**, **J**) Quantification of the TEM examination for the sciatic nerve at 24-mo. There were three mice in each group; 3–5 micrographs (5000×) for each mouse were examined. (**K**, **L**) Quantification of the TEM examination for the optic nerve at 24-mo. There were three mice in each group; 10 micrographs (10 000×) for each mouse were examined. All results are mean ± SD. $^{*}P < 0.05$; $^{**}P < 0.005$.

in a loss-of-function KO mouse study. Here, we provide further evidence using a gain-of-function study involving TG mice that demonstrates how an increase in the level of Cisd2 protein during middle and old age is able to delay aging and extends healthy lifespan.

To test whether the *Pol II-Cisd2* transgene can complement the mutation in Cisd2 KO mice, we generated Cisd2 TG mice (line A161; TG/+ hemizygous) carrying an endogenous Cisd2 KO (−/−) background, namely Cisd2 TG;KO mice (Supplementary Material, Fig. S6A). Importantly, our results revealed that the transgene was able to partially rescue the premature aging phenotype compared with Cisd2 KO mice, in particular, with respect to degeneration of skeletal muscle (Supplementary Material, Fig. S6B–G), cardiac muscle (Supplementary Material, Fig. S6H–J) and the sciatic nerve (Supplementary Material, Fig. S6K–M), as well as body weight (Supplementary Material, Fig. S6N). It should be noted that the level of protein expression of the transgene is very low (Fig. 1). These results provide strong evidence that the *Pol II-Cisd2* transgene can functionally complement, at least in part, the

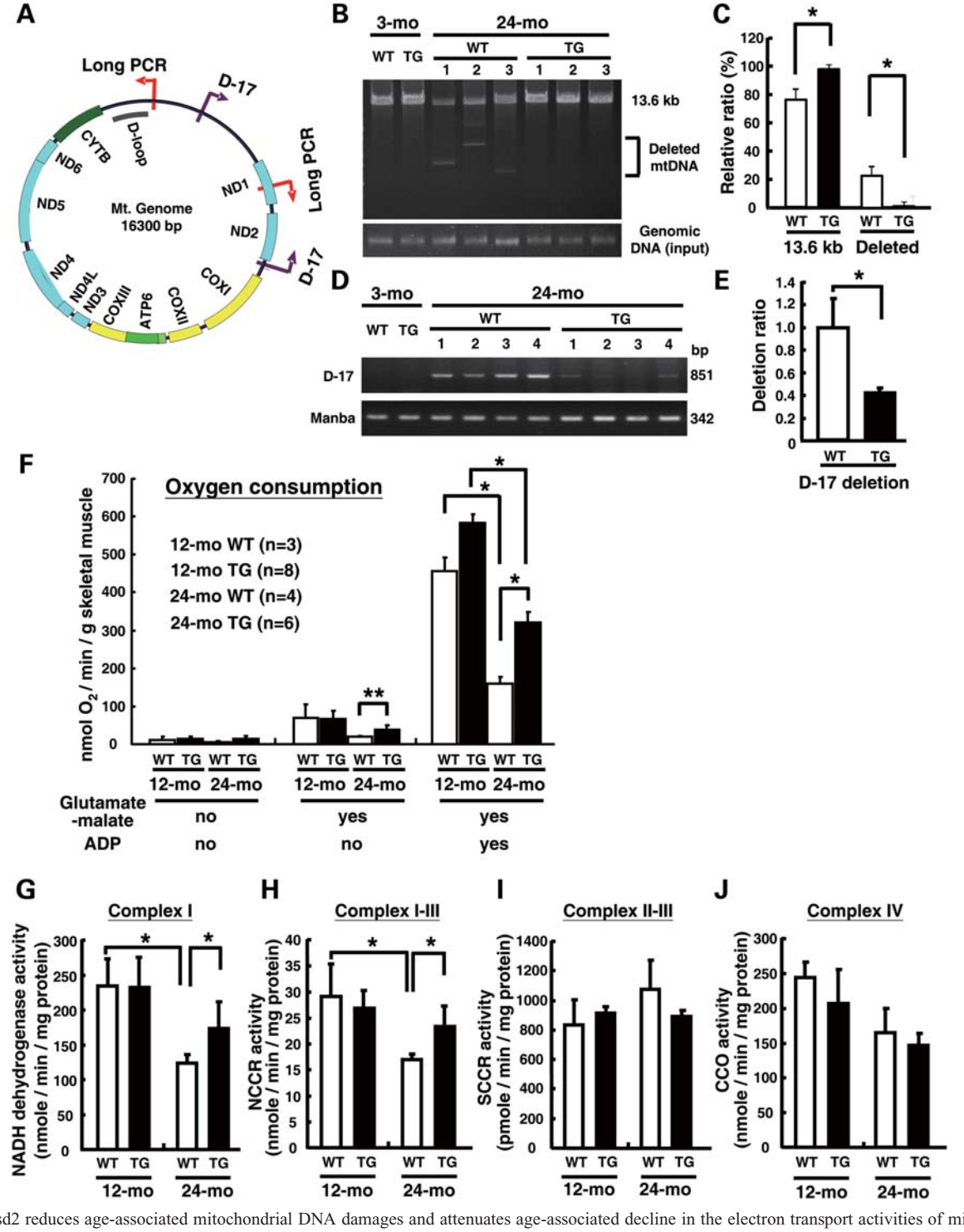

Figure 5. Cisd2 reduces age-associated mitochondrial DNA damages and attenuates age-associated decline in the electron transport activities of mitochondria. (**A**) Map of the mtDNA genome and the positions of primer pairs used to detect deletions. ND1, NADH dehydrogenase subunit 1; COXI, cytochrome *c* oxidase subunit I; ATP6, ATP synthase F0 subunit 6; CYTB, cytochrome *b*. (**B**) Long PCR (13.6 kb) of mtDNA fragment using genomic DNA isolated from skeletal muscle. (**C**) Comparison of the relative percentage of 13.6-kb long PCR product and deleted mtDNA PCR signals between WT and Cisd2 TG mice at 24-mo. (**D**) PCR detection of the D-17 deletion using genomic DNA isolated from skeletal muscle. Manba is a nuclear-encoded protein. (**E**) Comparison of the relative levels of D-17 deletion between WT and Cisd2 TG mice at 24-mo. (**F**) Respiratory activity of isolated mitochondria expressed as oxygen consumption rate in the resting state for glutamate–malate supported respiration and for ADP-activated respiration. (**G**) Measurement of NADH dehydrogenase activity, which represents Complex I, in the skeletal muscles. (**H**) Measurement of NCCR activity, which represents electron transport activity from Complex I to III, in the skeletal muscles. (**I**) Measurement of SCCR activity, which represents electron transport activity from Complexes II to III, in the skeletal muscles. (**J**) CCO activity, which represents Complex IV, in the skeletal muscles. In (G)–(J), there were four animals for each group of mice. All results are mean ± SD. $^{*}P < 0.05$; $^{**}P < 0.005$.

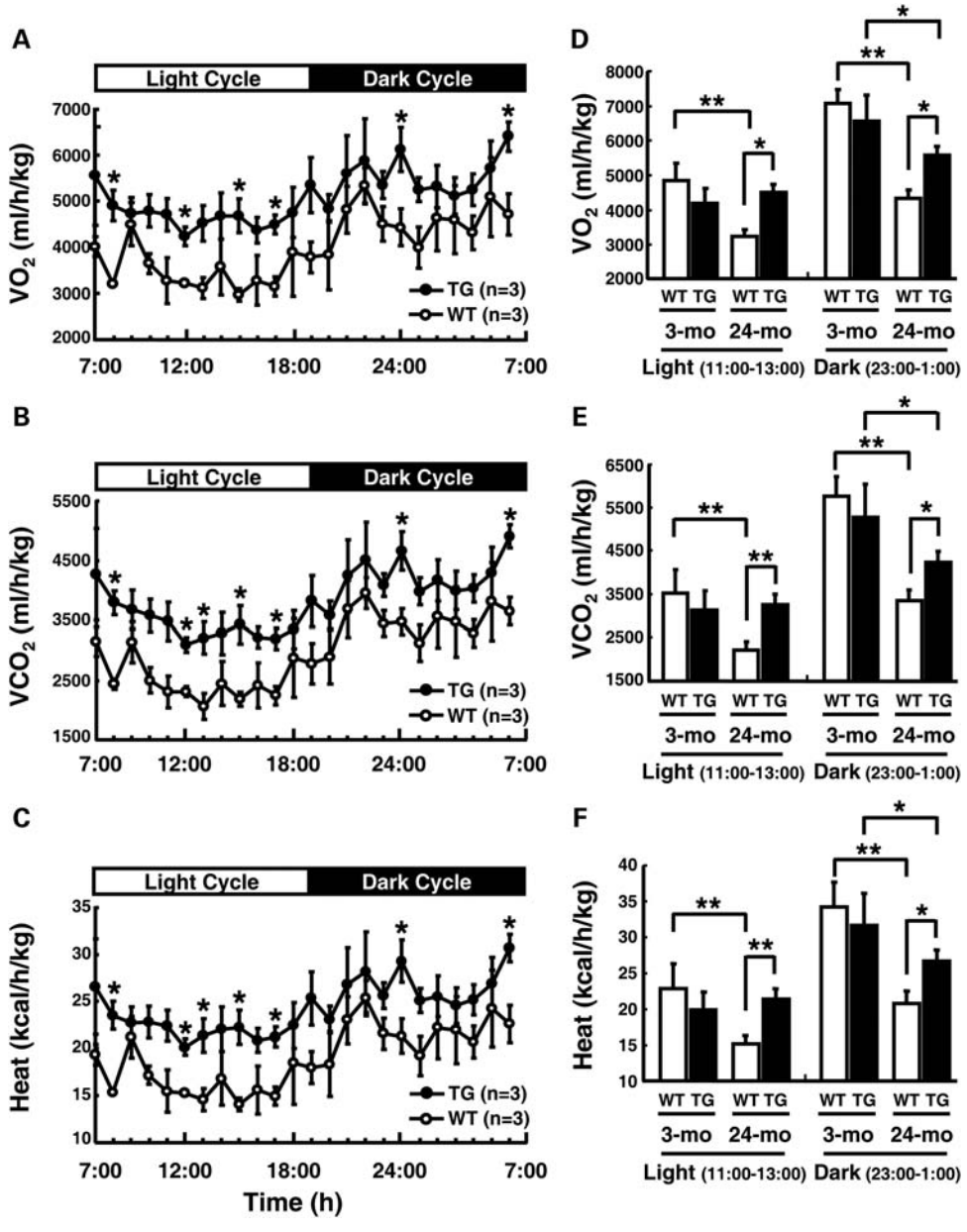

Figure 6. Cisd2 reduces the age-associated decline in whole-body energy metabolism. (**A**–**C**) Hour-to-hour average of whole-body oxygen consumption (VO_2) (A), CO_2 production (VCO_2) (B) and heat generation (C) during the light and dark periods for 24-mo WT and Cisd2 TG mice. (**D**–**F**) Quantification of whole-body VO_2 (D), VCO_2 (E) and heat generation (F) during the light and dark periods, and comparison between WT and Cisd2 TG mice at 3-mo and 24-mo. In (D)–(F), the quantification results were calculated using data collected during the middle of the light period (11:00–13:00) and during the middle of the dark period (23:00–1:00). All results are mean ± SD. $^{*}P < 0.05$; $^{**}P < 0.005$.

mutant phenotype of Cisd2 KO mice, and that the long-lived phenotype is not due to any non-Cisd2-associated mutation in the TG mouse line.

In this study, we generated two independent TG mouse lines, A161 and A214, containing the *Pol II-Cisd2* TG construct. All of the results presented in the figures and table of this article were prepared from line A161. Line A214 was created 2 years after the establishment of line A161 when the line A161 began to exhibit a delay in the aging process. The second line was created in order to ascertain whether the anti-aging phenotype mediated by Cisd2 in line A161 could be reproduced in a second independent TG mouse line (Supplementary Material, Fig. S7A); therefore, we have also performed a phenotypic characterization of the line A214. The survival rate of line A214 has been followed for 30 months and the survival curves for both males and females of line A214 have begun to separate from those of the WT controls and these mice are also exhibiting signs of a longer lifespan (Supplementary Material, Fig. S7B and C). Importantly, our results reveal that Cisd2 is also able to protect mice against age-associated degeneration in skeletal muscle, mitochondrial structures and neurons of sciatic and optic nerves

in this second TG line, A214 (Supplementary Material, Fig. S7D–O).

In summary, maintenance of a persistent expression level of Cisd2 over the whole life, when achieved by TG expression, protects mice from age-associated mitochondrial damage in terms of both genomic DNA and at the ultrastructural level as well as attenuating age-associated functional decline with respect to energy metabolism and oxidative phosphorylation of mitochondria. At the organism level, this protection mediated by Cisd2 contributes to the alleviation of age-associated phenotypic changes in multiple tissues including skin, muscle and neurons. Additionally, Cisd2 helps to preserve whole-body energy metabolism in the TG mice. Together, these changes give the mice a long-lived phenotype that is linked to an extension in healthy lifespan and a delay in age-associated diseases.

The lifespan extension of Cisd2 TG mice (19–20%) is similar in magnitude to that found for MCAT mice (17–21%), which overexpress human catalase targeted to the mitochondria (28), but less than that achieved by caloric restriction (30–50%), dwarfism (26–68%) or that observed in other genetic models of delayed and decelerated aging (13,29). However, the promoting effect of Cisd2 on lifespan is accompanied by no apparent deleterious side effects on growth, fertility, food intake and metabolism. Prolongation of Cisd2 expression into middle and old age seems to have no obvious negative effect that is detrimental to the whole organism. Regarding lifespan extension in mammals, the most striking prolongation has been reported for the dwarf mice. For example, Ames dwarf mice are remarkably long-lived and outlive their WT controls by 49–68% and exhibit many phenotypic characteristics related to a delay in aging. However, these dwarf mice have a genetic deficit in the growth hormone signaling pathway that leads to a phenotype involving severe growth retardation (dwarfism), sterility or reduced fertility and impaired anterior pituitary development/function (30). In terms of reproduction, there seems to be generally a reverse correlation between reproduction and lifespan. Most long-lived mutant mice show delayed reproductive development and a significantly reduced fertility (13). In addition to the dwarf mice having severely reduced fertility, the long-lived Klotho TG mice, which develop normally and outlived by 19–31% their normal littermates, also display reduced fecundity (16). In contrast to these earlier findings on extending the lifespan of mice, our TG mouse study provides strong evidence to indicate that persistent expression of Cisd2 is able to extend healthy lifespan without any detectable deficit in development and physiological functioning.

In addition to mouse studies, human genetic investigations will form an essential part of uncovering the physiological functions of the CISD2 protein. When used together, human and mouse genetic studies will be able to provide evidence as to whether *CISD2* is a ‘master gene’ for extreme old age (31). Accordingly, it will be of great interest to examine CISD2 expression levels in various human populations during the aging process and specifically to identify polymorphisms in the DNA sequence and compare gene activity and/or protein function between normal populations and long-lived centenarian groups. In addition, a detailed exploration of the potential control sequences in the upstream/downstream that might affect Cisd2 expression will help to establish why and how Cisd2 expression becomes reduced with age in mice. The *Cisd2* gene is conserved across a very wide range of species and is very highly conserved in mammals (Supplementary Material, Fig. S8). This implies two things. Firstly, because mutation in human *CISD2* gene is highly deleterious (3), it is unlikely that genetic variation in the coding sequence is the source of differences in lifespan across human and other populations. Secondly, because the Cisd2 KO mice (7) showed a significantly shorter lifespan with premature aging, but not a drastically shorter one, it implies that Cisd2 may not directly control lifespan in mammals, but rather its expression level indirectly affects lifespan and quality of life. In this context, control of expression of Cisd2 becomes important to extending lifespan. The Cisd2 TG mouse results thus provide an experimental basis that will help the development of a regimen that may stimulate human CISD2 expression and/or activity in order to ameliorate age-associated phenotypes such as muscle and neuronal tissue degeneration and thus possibly extend the healthy lifespan of humans.

MATERIALS AND METHODS

Generation of the Cisd2 TG mice

The mouse *Cisd2* coding region was created such that it was driven by the RNA polymerase II large subunit promoter (Pol II; NCBI Accession M14101 bases 1–712). The 0.33-kb synthetic intron and the 0.28-kb bovine growth hormone polyA signal (pA) were derived from the pIRES-EGFP plasmid (CLONTECH #6064-1). Two direct repeats of the chicken HS4 insulator (NCBI Accession U78775 bases 10–1199) were placed downstream of the polyA signal to block positional effects. The Cisd2 TG mice were generated by pronucleus microinjection of C57BL/6 fertilized eggs. There are two independent TG mouse lines A161 and A214; line A214 was created 2 years after the establishment of line A161. Both lines of the Cisd2 TG mice have a C57BL/6 background. The genotypes of the mice were determined by PCR using tail DNA. The mice were bred in a specific pathogen-free facility; the animal protocol was approved by the Institutional Animal Care and Use Committee of the National Yang-Ming University.

RNA analysis

Total RNA was isolated from mouse tissue using TRIzol Reagent (Life Technology). Northern blot hybridization was performed as described previously (32). We execute real-time quantitative PCR using a Roche LightCycler 480 Real-time PCR instrument, and a TaqMan probe obtained from the Universal ProbeLibrary (Roche Applied Science) and LightCycler TaqMan Master (Roche Applied Science). All amplifications were carried out in triplicate for each RNA sample and primer set. All real-time quantitative PCR measurements were done using RNA samples from three individual mice. The amount of total input cDNA was normalized using hypoxanthine-guanine phosphoribosyltransferase as an internal control.

Western blotting

The preparation of rabbit anti-mouse Cisd2 polyclonal antibody and western blot analysis have been described previously (7); glyceraldehyde 3-phosphate dehydrogenase (1:5000; Abcam ab9482) was used as an internal control for the western blot analysis.

Histopathology

Various mouse tissues were collected, fixed with 10% formalin buffered with phosphate and embedded in paraffin. Tissue sections (3–4 μm) were subjected to hematoxylin&eosin (H&E) and Masson's trichrome staining by standard procedures (33).

Immunohistochemistry staining

Immunohistochemistry (IHC) staining for perilipin was performed using paraffin-embedded skeletal muscle sections (3 μm). Muscle sections were soaked in antigen retrieval buffer containing 10 mM sodium citrate (pH 6.0) and heated in a microwave oven for 2 × 10 min (Sunpentown SM-1220, 650 W). The sections were then incubated with primary antibody against perilipin (1:100, Cell Signaling D418 rabbit polyclonal antibody) at 4°C for 18–24 h and detected by secondary antibody (Invitrogen Flour 570-conjugated goat anti-rabbit antibody). The sections were visualized by fluorescence microscope (OLYPUS BX51) and then the pictures were captured with DP Controller Ver. 3.1.1.267 software. Nuclei were counterstained with 4′-6-diamidino-2-phenylindole (DAPI; Sigma).

Transmission electron microscopy

Various mouse tissues were fixed in a mixture of glutaraldehyde (1.5%) and paraformaldehyde (1.5%) in phosphate buffer at pH 7.3. They were post-fixed in 1% OsO_4, 1.5% potassium hexanoferrate, then rinsed in cacodylate and 0.2 M sodium maleate buffers (pH 6.0) followed by block-staining with 1% uranyl acetate. Following dehydration, the various tissues were embedded in Epon and sectioned for TEM as described previously (34).

Water repulsion

Mice were immersed in 37°C water bath for 3 min and placed on a paper towel to absorb excess water. Next, the mice were exposed to ambient temperature and their body weight and temperature recorded from 5 to 60 min after water immersion (18). The body temperature was detected by Microcomputer Thermometer MODEL 7000H (Jenco Electronics Ltd).

Muscle strength

Grip strength of the forelimbs was determined using Popular Model Digital Force Gauge (DS2, IMADA Co., Ltd). Peak gripping force at the point of grip failure was recorded as grip strength. Each mouse performed 10 trials with 15 s of rest between each trial (35,36). There were more than three mice in each group, and three independent measurements were carried out for each mouse.

Open-field locomotion and rotarod trials

Open-field activity test was used to monitor the motor activity, exploratory and anxiety oriented by the true scan photo beam tracking system (Coulbourn Instruments); this system includes an arena, sensor rings and interface lines. Individual mouse was placed in the arena, and behavior was recorded for 60 min. Spontaneous locomotor activity, olfactory activity (rearing and sniffing movements) and stereotypical movements were gauged (37–39). Rotarod was used to analyze the motor coordination, balance and exhaustion resistance using Rotarod treadmill (Singa Technology Corporation). The mice were placed on a rotating rod running at different speeds and durations. The sensor on the bottom of the apparatus can record when mice fall down from the rotating rod. Mice were pre-trained for 3 days and trained for 4 times per day on 3 consecutive days. Each training held for 90 s with a steady speed of 12 rpm. Subsequently, there were three conditions for trials: test 1 (T1) 90-s trial at a steady speed of 33 rpm; test 2 (T2), 90-s trial at a steady speed of 40 rpm; and test 3 (T3), 600-s trial at a steady speed of 15 rpm (39,40).

Mitochondrial DNA deletion

Long PCR (13.6 kb) of mtDNA fragment for monitoring the integrity of mitochondrial genome was performed using genomic DNA isolated from skeletal muscle (23). The primers for the long PCR were: 5′-GCCAGCCTGACCC ATAGCCATAATAT-3′ and 5′-ATTAATAAGGCCAGGAC CAAACCT-3′. The relative percentage of the 13.6-kb long PCR and deleted mtDNA PCR signals was compared between WT and Cisd2 TG mice. PCR detection of the D-17 deletion was performed using genomic DNA isolated from skeletal muscle as described previously (24).

D-loop oxidative damage

Oxidative damage of the D-loop of mtDNA was determined by monitoring the content of 8-OHdG (41). Genomic DNA isolated from skeletal muscle was treated with 8-hydroxyguanine DNA-glycosylase (OGG1) to remove 8-OHdG residues and form an apurine site in the DNA template. As the proportion of 8-OHdG in mtDNA increases, there is less intact mtDNA left after OGG1 digestion and this leads to a lower yield of PCR product. Each sample of 500 ng DNA was first treated with or without 1 unit of OGG1 at 37°C for 1 h and these two groups of DNA were both amplified by quantitative real-time PCR using D-loop specific primers. The level of mtDNA D-loop damage was then calculated as the efficiency of amplification of the OGG1-treated DNA group relative to that of the untreated DNA group.

Measurement of mitochondrial oxygen consumption

Mitochondria were isolated from mouse tissues as previously described (7). The oxygen consumption rate was measured

using a 782 Oxygen Meter (Strathkelvin Instruments, Scotland, UK). An aliquot of 300 μl assay buffer (125 mM sucrose, 65 mM KCl, 2 mM $MgCl_2$, 20 mM Na^+, K^+-phosphate buffer, pH 7.2) containing about 75 μg of mitochondria was delivered into the closed chamber of the oxygen meter at 37°C in order to measure the steady-state oxygen consumption rate of the mitochondria (42). To further estimate the respiratory function of the mitochondria, we added 10 mM glutamate/malate (Sigma-Aldrich) as well as 1 mM adenosine diphosphate (ADP) in that order and measured the rate simultaneously after each step. Finally, the oxygen consumption rate of isolated mitochondria was normalized against the weight of skeletal muscle.

Respiratory enzyme complex activity

The activity of the nicotinamide adenine dinucleotide (NADH) dehydrogenase of Complex I was measured by following the reduction of potassium ferricyanide as described previously (43). Total protein lysate was extracted from skeletal muscle and incubated with the assay mixture (2 mM KCN, 0.5 mM β-NADH, 20 mM K_2HPO_4 at pH 7.4). After addition of $K_3Fe(CN)_6$ to the mixture, the change in the absorbance at 420 nm was recorded on a UV/visible spectrophotometer. Rotenone, a specific Complex I inhibitor, was then added to the reaction in order to measure the NADH dehydrogenase activity excluding Complex I. By subtracting this from total activity, the Complex I activity was obtained. The activity assays for Complexes I–III, Complexes II and III and Complex IV were performed as described previously (7,44).

Whole-body energy metabolism

Whole-body energy metabolism was measured by indirect calorimetry. A TSE Calorimetry Module of the LabMaster System was used and is able to determine the oxygen consumption rate (VO_2), carbon dioxide production rate (VCO_2) and energy expenditure (heat) of small laboratory animals. Individual mice were monitored over 24 h by indirect calorimetry using this system (45).

Intracellular GSH level

The content of total reduced GSH was measured by the Bioxytech GSH/GSSG-412TM Kit (Oxis Research) according to the manufacturer's instructions. Briefly, weighted skeletal muscles were homogenated in 5% metaphoric acid (MPA) and centrifuged at 10 000*g* for 15 min at 4°C. The MPA extract was diluted and then incubated with the mixture containing 5-5′-dithiobis-2-nitrobenzoic acid, nicotinamide adenine dinucleotide and glutathione reductase. The change of absorbance at 412 nm within 3 min was measured at room temperature using a spectrophotometer for both samples and standards (0–3.0 μM GSH).

Statistics

Results are presented as mean ± SD. Comparisons between two groups were carried out using Student's *t*-test. Mouse survival rates were calculated by the Kaplan–Meier method, and the differences in the survival of the different groups of mice were determined by the log-rank (Mental–Cox) test. When analyzing statistical differences between different groups of mice, $P < 0.05$ was considered significant.

SUPPLEMENTARY MATERIAL

Supplementary Material is available at *HMG* online.

ACKNOWLEDGEMENTS

We thank Chia-Hui Chen, Hou-Wen Chou and Yao-Kuan Huang for their technical assistance. We thank the Taiwan Mouse Clinic, and the Microarray and Gene Expression Analysis Core Facility of the National Yang-Ming University Genome Research Center; the Core Facilities are supported by National Science Council.

Conflict of Interest statement. None declared.

FUNDING

This work was supported by the National Science Council (grant number NSC97-2320-B-010-015-MY3, NSC99-2628-B-010-001-MY3 and NSC100-2320-B-010-026-MY3 to T.F.T.), Aging and Health Research Center, National Yang-Ming University and a grant from the Ministry of Education, Aim for the Top University Plan to T.F.T.

REFERENCES

1. Puca, A.A., Daly, M.J., Brewster, S.J., Matise, T.C., Barrett, J., Shea-Drinkwater, M., Kang, S., Joyce, E., Nicoli, J., Benson, E. *et al.* (2001) A genome-wide scan for linkage to human exceptional longevity identifies a locus on chromosome 4. *Proc. Natl Acad. Sci. USA*, **98**, 10505–10508.
2. Chen, Y.F., Wu, C.Y., Kirby, R., Kao, C.H. and Tsai, T.F. (2010) A role for the CISD2 gene in life span control and human disease. *Ann. NY Acad. Sci.*, **1201**, 58–64.
3. Amr, S., Heisey, C., Zhang, M., Xia, X.J., Shows, K.H., Ajlouni, K., Pandya, A., Satin, L.S., El-Shanti, H. and Shiang, R. (2007) A homozygous mutation in a novel zinc-finger protein, ERIS, is responsible for Wolfram syndrome 2. *Am. J. Hum. Genet.*, **81**, 673–683.
4. Conlan, A.R., Axelrod, H.L., Cohen, A.E., Abresch, E.C., Zuris, J., Yee, D., Nechushtai, R., Jennings, P.A. and Paddock, M.L. (2009) Crystal structure of Miner1: the redox-active 2Fe–2S protein causative in Wolfram Syndrome 2. *J. Mol. Biol.*, **392**, 143–153.
5. Chang, N.C., Nguyen, M., Germain, M. and Shore, G.C. (2010) Antagonism of Beclin 1-dependent autophagy by BCL-2 at the endoplasmic reticulum requires NAF-1. *EMBO J.*, **29**, 606–618.
6. Chang, N.C., Nguyen, M., Bourdon, J., Risse, P.A., Martin, J., Danialou, G., Rizzuto, R., Petrof, B.J. and Shore, G.C. (2012) Bcl-2-associated autophagy regulator Naf-1 required for maintenance of skeletal muscle. *Hum. Mol. Genet.*, **21**, 2277–2287. [Epub ahead of print].
7. Chen, Y.F., Kao, C.H., Chen, Y.T., Wang, C.H., Wu, C.Y., Tsai, C.Y., Liu, F.C., Yang, C.W., Wei, Y.H., Hsu, M.T. *et al.* (2009) Cisd2 deficiency drives premature aging and causes mitochondria-mediated defects in mice. *Genes Dev.*, **23**, 1183–1194.
8. Chen, Y.F., Kao, C.H., Kirby, R. and Tsai, T.F. (2009) Cisd2 mediates mitochondrial integrity and life span in mammals. *Autophagy*, **5**, 1043–1045.
9. Kuro-o, M., Matsumura, Y., Aizawa, H., Kawaguchi, H., Suga, T., Utsugi, T., Ohyama, Y., Kurabayashi, M., Kaname, T., Kume, E. *et al.* (1997) Mutation of the mouse *klotho* gene leads to a syndrome resembling ageing. *Nature*, **390**, 45–51.

10. Hasty, P., Campisi, J., Hoeijmakers, J., van Steeg, H. and Vijg, J. (2003) Aging and genome maintenance: lessons from the mouse? *Science*, **299**, 1355–1359.
11. Mounkes, L.C., Kozlov, S., Hernandez, L., Sullivan, T. and Stewart, C.L. (2003) A progeroid syndrome in mice is caused by defects in A-type lamins. *Nature*, **423**, 298–301.
12. Niedernhofer, L.J., Garinis, G.A., Raams, A., Lalai, A.S., Robinson, A.R., Appeldoorn, E., Odijk, H., Oostendorp, R., Ahmad, A., van Leeuwen, W. *et al.* (2006) A new progeroid syndrome reveals that genotoxic stress suppresses the somatotroph axis. *Nature*, **444**, 1038–1043.
13. Chen, Y.F., Wu, C.Y., Kao, C.H. and Tsai, T.F. (2010) Longevity and life span control in mammals: lessons from the mouse. *Ageing Res. Rev.*, **9S**, S28–S35.
14. Le Bourg, E. (2007) Does reproduction decrease longevity in human beings? *Ageing Res. Rev.*, **6**, 141–149.
15. Mitteldorf, J. (2010) Female fertility and longevity. *Age (Dordr)*, **32**, 79–84.
16. Kurosu, H., Yamamoto, M., Clark, J.D., Pastor, J.V., Nandi, A., Gurnani, P., McGuinness, O.P., Chikuda, H., Yamaguchi, M., Kawaguchi, H. *et al.* (2005) Suppression of aging in mice by the hormone Klotho. *Science*, **309**, 1829–1833.
17. Jasienska, G. (2009) Reproduction and lifespan: trade-offs, overall energy budgets, intergenerational costs, and costs neglected by research. *Am. J. Hum. Biol.*, **21**, 524–532.
18. Chen, H.C., Smith, S.J., Tow, B., Elias, P.M. and Farese, R.V. Jr. (2002) Leptin modulates the effects of acyl CoA:diacylglycerol acyltransferase deficiency on murine fur and sebaceous glands. *J. Clin. Invest.*, **109**, 175–181.
19. Thody, A.J. and Shuster, S. (1989) Control and function of sebaceous glands. *Physiol. Rev.*, **69**, 383–416.
20. Delmonico, M.J., Harris, T.B., Visser, M., Park, S.W., Conroy, M.B., Velasquez-Mieyer, P., Boudreau, R., Manini, T.M., Nevitt, M., Newman, A.B. *et al.* (2009) Longitudinal study of muscle strength, quality, and adipose tissue infiltration. *Am. J. Clin. Nutr.*, **90**, 1579–1585.
21. Goodpaster, B.H., Kelley, D.E., Thaete, F.L., He, J. and Ross, R. (2000) Skeletal muscle attenuation determined by computed tomography is associated with skeletal muscle lipid content. *J. Appl. Physiol.*, **89**, 104–110.
22. Rivas, D.A., Morris, E.P. and Fielding, R.A. (2011) Lipogenic regulators are elevated with age and chronic overload in rat skeletal muscle. *Acta Physiol. (Oxf)*, **202**, 691–701.
23. Santos, J.H., Meyer, J.N., Mandavilli, B.S. and Van Houten, B. (2006) Quantitative PCR-based measurement of nuclear and mitochondrial DNA damage and repair in mammalian cells. *Methods Mol. Biol.*, **314**, 183–199.
24. Tanhauser, S.M. and Laipis, P.J. (1995) Multiple deletions are detectable in mitochondrial DNA of aging mice. *J. Biol. Chem.*, **270**, 24769–24775.
25. Petrosillo, G., Matera, M., Moro, N., Ruggiero, F.M. and Paradies, G. (2009) Mitochondrial complex I dysfunction in rat heart with aging: critical role of reactive oxygen species and cardiolipin. *Free Radic. Biol. Med.*, **46**, 88–94.
26. Stefanatos, R. and Sanz, A. (2011) Mitochondrial complex I: a central regulator of the aging process. *Cell Cycle*, **10**, 1528–1532.
27. Rebrin, I. and Sohal, R.S. (2008) Pro-oxidant shift in glutathione redox state during aging. *Adv. Drug Deliv. Rev.*, **60**, 1545–1552.
28. Schriner, S.E., Linford, N.J., Martin, G.M., Treuting, P., Ogburn, C.E., Emond, M., Coskun, P.E., Ladiges, W., Wolf, N., Van Remmen, H. *et al.* (2005) Extension of murine life span by overexpression of catalase targeted to mitochondria. *Science*, **308**, 1909–1911.
29. Fontana, L., Partridge, L. and Longo, V.D. (2010) Extending healthy life span—from yeast to humans. *Science*, **328**, 321–326.
30. Bartke, A. and Brown-Borg, H. (2004) Life extension in the dwarf mouse. *Curr. Top. Dev. Biol.*, **63**, 189–225.
31. Strauss, E. (2001) Longevity: hints of a 'master gene' for extreme old age. *Science*, **293**, 1570–1571.
32. Sambrook, J. and Russell, D.W. (2001) *Molecular Cloning: A Laboratory Manual*. Cold Spring Harbor Laboratory Press, Cold Spring Harbor, NY.
33. Young, B. and Heath, J.W. (2003) *Wheater's Functional Histology: A Text and Colour Atlas*. Churchill Livingstone, London.
34. Kao, C.H., Chen, J.K., Kuo, J.S. and Yang, V.C. (1995) Visualization of the transport pathways of low density lipoproteins across the endothelial cells in the branched regions of rat arteries. *Atherosclerosis*, **116**, 27–41.
35. MacArthur, D.G., Seto, J.T., Chan, S., Quinlan, K.G., Raftery, J.M., Turner, N., Nicholson, M.D., Kee, A.J., Hardeman, E.C., Gunning, P.W. *et al.* (2008) An Actn3 knockout mouse provides mechanistic insights into the association between alpha-actinin-3 deficiency and human athletic performance. *Hum. Mol. Genet.*, **17**, 1076–1086.
36. Loy, R.E., Orynbayev, M., Xu, L., Andronache, Z., Apostol, S., Zvaritch, E., MacLennan, D.H., Meissner, G., Melzer, W. and Dirksen, R.T. (2011) Muscle weakness in Ryr1I4895T/WT knock-in mice as a result of reduced ryanodine receptor Ca^{2+} ion permeation and release from the sarcoplasmic reticulum. *J. Gen. Physiol.*, **137**, 43–57.
37. Wilson, R.C., Vacek, T., Lanier, D.L. and Dewsbury, D.A. (1976) Open-field behavior in muroid rodents. *Behav. Biol.*, **17**, 495–506.
38. Kwon, C.H., Luikart, B.W., Powell, C.M., Zhou, J., Matheny, S.A., Zhang, W., Li, Y., Baker, S.J. and Parada, L.F. (2006) Pten regulates neuronal arborization and social interaction in mice. *Neuron*, **50**, 377–388.
39. Wu, W.L., Lin, Y.W., Min, M.Y. and Chen, C.C. (2010) Mice lacking Asic3 show reduced anxiety-like behavior on the elevated plus maze and reduced aggression. *Genes Brain Behav.*, **9**, 603–614.
40. Carter, R.J., Morton, J. and Dunnett, S.B. (2001) Motor coordination and balance in rodents. *Curr. Protoc. Neurosci.*, **8**, 12.1–12.4.
41. Lin, C.S., Wang, L.S., Tsai, C.M. and Wei, Y.H. (2008) Low copy number and low oxidative damage of mitochondrial DNA are associated with tumor progression in lung cancer tissues after neoadjuvant chemotherapy. *Interact. Cardiovasc. Thorac. Surg.*, **7**, 954–958.
42. Chen, C.T., Shih, Y.R., Kuo, T.K., Lee, O.K. and Wei, Y.H. (2008) Coordinated changes of mitochondrial biogenesis and antioxidant enzymes during osteogenic differentiation of human mesenchymal stem cells. *Stem Cell*, **26**, 960–968.
43. Lu, F., Selak, M., O'Connor, J., Croul, S., Lorenzana, C., Butunoi, C. and Kalman, B. (2000) Oxidative damage to mitochondrial DNA and activity of mitochondrial enzymes in chronic active lesions of multiple sclerosis. *J. Neurol. Sci.*, **177**, 95–103.
44. Wei, Y.H., Lu, C.Y., Lee, H.C., Pang, C.Y. and Ma, Y.S. (1998) Oxidative damage and mutation to mitochondrial DNA and age-dependent decline of mitochondrial respiratory function. *Ann. NY Acad. Sci.*, **854**, 155–170.
45. Kuo, L.H., Tsai, P.J., Jiang, M.J., Chuang, Y.L., Yu, L., Lai, K.T. and Tsai, Y.S. (2011) Toll-like receptor 2 deficiency improves insulin sensitivity and hepatic insulin signaling in the mouse. *Diabetologia*, **54**, 168–179.